IOPscience iopscience.iop.org

Home Search Collections Journals About Contact us My IOPscience

Effect of ion-milled barriers on electron transport in micrometer-sized tunnel junctions

This content has been downloaded from IOPscience. Please scroll down to see the full text.

2014 J. Phys. D: Appl. Phys. 47 105305

(http://iopscience.iop.org/0022-3727/47/10/105305)

View the table of contents for this issue, or go to the journal homepage for more

Download details:

IP Address: 140.113.38.11
This content was downloaded on 28/04/2014 at 23:09

Please note that terms and conditions apply.

IOP Publishing Journal of Physics D: Applied Physics
J. Phys. D: Appl. Phys. **47** (2014) 105305 (5pp) doi:10.1088/0022-3727/47/10/105305

Effect of ion-milled barriers on electron transport in micrometer-sized tunnel junctions

Yen-Chi Lee[1], Yong-Han Lin[2], Jong-Ching Wu[1] and Juhn-Jong Lin[2,3]

[1] Department of Physics, National Changhua University of Education, Changhua 50058, Taiwan
[2] Institute of Physics, National Chiao Tung University, Hsinchu 30010, Taiwan
[3] Department of Electrophysics, National Chiao Tung University, Hsinchu 30010, Taiwan

E-mail: yonghanlin@gmail.com and phjcwu@cc.ncue.edu.tw

Received 17 November 2013, revised 30 December 2013
Accepted for publication 6 January 2014
Published 19 February 2014

Abstract

We studied the electron transport properties of micrometre-sized all-Al tunnel junctions (TJs) between 2 and 300 K, in which the AlO_x layer grown by O_2 plasma was moderately Ar-ion-milled prior to top electrode deposition. In contrast to the direct tunnelling in the TJs whose barriers are intact (not ion-milled), the zero-bias conductances and the current–voltage characteristics of the TJs as processed are found to be best described by the fluctuation-induced tunnelling conduction mechanism. This observation indicates the formation of nanoscopic incomplete pinholes in the AlO_x layer, owing to large junction–barrier interfacial roughness introduced by the ion-milling process. Topographical features revealed by the cross-sectional transmission electron microscopy imaging of the TJ stack conform to this result. This study is of relevance to cases in which ion-milling techniques are applied in tailoring the TJ properties.

Keywords: electron tunnelling, ion milling, interfacial roughness

(Some figures may appear in colour only in the online journal)

1. Introduction

Accelerated ion beams have long been utilized as a versatile tool in materials science. The method mainly finds use in applications such as thin film deposition and precision machining of fine structures, which depend on the physical removal of atoms from solids via the impact of energetic ions. Recently, the tool has been applied to modify [1–7] the barrier properties of tunnel junction (TJ) devices for use in magnetic storage [8] or electronics technologies [7]. An example is to fabricate TJs with selectable resistance–area products [5] or ultrathin barriers [2] through ion milling (etching) the barrier. In this respect, however, depending on the ion species and the beam parameters, ion bombardment has been observed to roughen the surface, resulting in a pronounced topography [9]. Energetic ions also likely penetrate into the material and consequently alter the material properties close to the surface [3, 4]. Employing accelerated ion beams in etching TJ barriers can therefore strongly affect the overall TJ transport behaviour, which is determined not only by the potential barrier shape but also by interfacial roughness [10–13], defect states in the barrier [14–16] and other types of disorder [17]. However, investigations thus far have focused on exploring the device functionality mostly around room temperature. No investigations of the transport properties spanning a wide temperature range for such TJs have been reported previously. These properties are no doubt crucial for the correct interpretation and evaluation of relevant TJ functionalities. Here, we investigate the effect of Ar-ion-milled barriers on electron transport in micrometre-sized TJs between 2 and 300 K. For simplicity, we study only all-Al ($Al/AlO_x/Al$) TJs in this work. We mention that, although nowadays epitaxial barrier materials (e.g., MgO) have been commonly used in the relevant fields, the convenient AlO_x barrier remains indispensable and could still well serve, especially in prototypical systems, for examining certain ideas [18] or issues [19] such as the effect we quest for in this study.

2. Experimental details

Our planar cross TJs were fabricated by electron-beam lithography, with the designed TJ area $A \approx 5 \times 5\,\mu m^2$. An

 © 2014 IOP Publishing Ltd Printed in the UK

electron cyclotron resonance ion shower system (ELIONIX EIS-220) was used to deposit the Al electrodes (sputtering) and also to grow and mill the insulating AlO_x layer. The AlO_x layer was grown on the surface of the bottom electrode for 2 min by applying O_2 plasma accelerated at 120 V with a current density of 0.02 mA cm^{-2} and a working pressure of 7 mPa, resulting in a thickness $d \approx 5$ nm. Prior to top electrode deposition, the AlO_x layer was exposed for $\approx$10 s to a shower of Ar ions accelerated at 340 V with a current density of 7.5 mA cm^{-2} and a working pressure of 8 mPa. The angle of incidence was $\sim$45° normal to the substrate. Immediately following this, the top electrode was deposited without breaking the vacuum. The TJ zero-bias conductances $G(T)$ and the current–voltage, $I(V)$, characteristics were measured in a Quantum Design Physical Properties Measurement System by a 4-probe method, with a Keithley K236 as the current source and a K2000 as the voltmeter. The cross-sectional transmission electron microscopy (TEM) images of the TJ stacks were taken by a JEOL JEM-2010 microscope.

3. Results and discussions

A total of 16 TJs with Ar-ion-milled barriers were made in four separate fabrication runs. The obtained $G(300\,\text{K})$ values are at least two orders of magnitude larger than those of the TJs whose barriers are intact (not ion-milled), as is expected when the barrier is thinned. Figure 1(*a*) shows the semi-log plot of the $G(T)$ behaviour for six of the TJs, from 2 to 300 K. For the 16 TJs, $G(300\,\text{K})$ was found to be distributed over a wide range ($G(300\,\text{K}) \approx 10^x\ \mu$S, where $-1 \leqslant x \leqslant 2$). The inset in figure 1(*a*) shows the number of TJs having an exponent x. The symbols next to each strip indicate the x values of the six TJs plotted in the main panel with the corresponding symbols. For these TJs, G decreases slowly as T decreases from 300 K. At $T \lesssim 150$ K, however, a more rapid (exponential-like) decrease appears and is more pronounced for the TJs with smaller $G(300\,\text{K})$ values. Below $T \approx 20$ K, G then appears to saturate. In Simmons' theory of direct (elastic) tunnelling [20], because of the thermal broadening of the Fermi–Dirac statistics, the $G(T)$ behaviour of a TJ with a barrier of *uniform* d has the form $G_S(T) \propto [1 + (T/T_S)^2]$, where T_S is a junction parameter. In this theory, an exponential-like decrease in G_S with decreasing T is not expected. To emphasize this, we plot in figure 1(*b*) the T^2 dependence of G normalized to $G(2\,\text{K})$ for the six TJs. It is clear that $G(T)$ significantly differs from the linear description of Simmons' model, which, by contrast, well describes the behaviour of a TJ with an intact barrier, as shown in figure 1(*c*).

Figures 2(*a*) and (*b*) show typical cross-sectional TEM images of the TJ stacks in which the AlO_x layers are intact and ion-milled, respectively. The intact barrier shows a nearly constant $d \approx 5$ nm while slightly undulating between the Al electrodes. On the other hand, the ion-milled barrier (figure 2(*b*)) is found to exhibit a more drastic spatial variation in d, which has been reduced to $\approx$2 nm (on average). This wrinkle-like structure (i.e. large junction-barrier interfacial roughness) can be understood as a result of several simultaneous kinetic motions of diffusing atoms or minute clusters at the surface upon ion bombardment

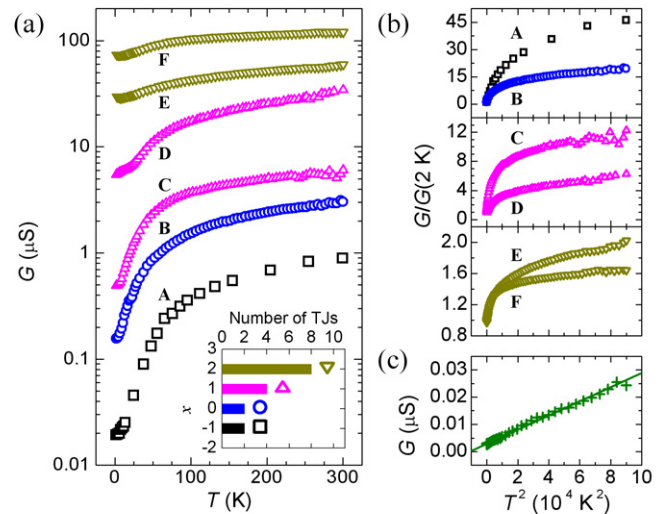

Figure 1. (*a*) Log G versus T and (*b*) $G/G(2\,\text{K})$ versus T^2 for TJs with ion-milled barriers. In (*a*), the data for TJs C and E are both divided by 10 for clarity. Inset: a histogram of the number of TJs having an exponent x ($G(300\,\text{K}) \approx 10^x\ \mu$S). (*c*) G versus T^2 for a TJ with an intact barrier. The straight line is the fit to Simmons' theory of tunnelling.

[9, 21]. The homogeneity and the ordering of the topography could possibly be controlled via proper selections of process parameters, which lie beyond the scope of this work. Considering electron transport, figure 2(*b*) suggests the possible occurrence of nanoscopic pinhole-like structures in such a *fractal* barrier when d varies considerably. If pinholes exist, they can short the electrodes and cause $G(T)$ to display a metallic feature, which is obviously not seen here. However, if pinholes are close to formation, these *incomplete* pinholes (or hot spots, i.e. the sharp points of closest approach between the two large conducting electrodes) that largely concentrate the tunnel current [11, 12] would also play a predominant role in the overall $G(T)$ behaviour [13]. That is, since practically all the tunnelling events occur at these incomplete pinholes, the size effect [22, 23] brought about by these very sharp points could actually dictate the entire junction property. This is an important issue commonly overlooked in previous studies.

In this case, due to the presence of thermal energy k_BT and the small capacitance C_e of the hot spot of an effective junction area A_e (where k_B is the Boltzmann constant, $C_e \propto A_e$, and $A_e \ll A$), the resulting random thermal fluctuation voltage $V_t = \pm(k_BT/C_e)^{1/2}$ across the insulating gap at the hot spot will be exceedingly large. (Note that C_e is only a very small part of the total capacitance C of the junction.) This in turn can substantially lower and narrow the effective potential barrier shape seen by the electrons, giving an overall $G_F(T)$ behaviour accounted for by the so-called fluctuation-induced tunnelling conduction (FITC) mechanism [22, 23]. In this model, G_F decreases exponentially when T decreases. Due to the gradually vanishing V_t with decreasing T, G_F finally becomes much less dependent on T (i.e. G_F is saturated and recovers the elastic tunnelling behaviour when $T \to 0$). This behaviour is similar to that in our TJs shown in figure 1(*a*). In the following, we discuss our data in terms of the FITC model and show that the observed $G(T)$ behaviour can indeed be best described by it.

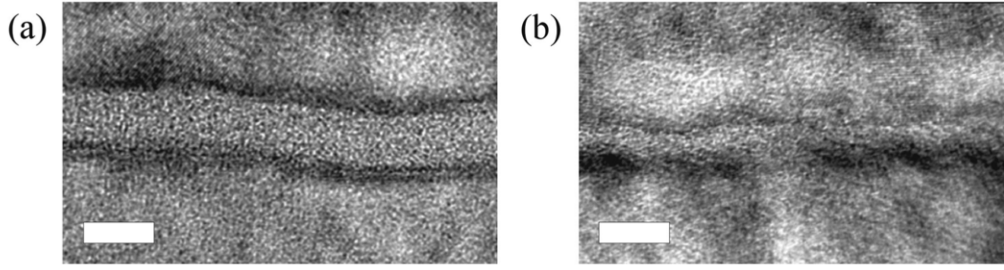

Figure 2. Cross-sectional TEM images of the TJ stacks whose barriers are (*a*) intact and (*b*) ion-milled. The scale bars are 5 nm.

As shown previously [13, 24], justifying the relevance of the FITC mechanism may be achieved by comparing two sets of characteristic parameter values determined independently of either the low bias voltage or the high bias voltage regimes of the measured $I(V)$ curves.

(i) At low bias voltages (i.e. the ohmic $I(V)$ regime), $G_F(T)$ in the FITC theory takes the form [22, 23]

$$G_F(T) = G_{F\infty} \exp[-T_1/(T_0 + T)], \qquad (1)$$

where the parameter $G_{F\infty}$ depends only weakly on T, and the characteristic energy scales $k_B T_1$ ($\propto A_e \phi^2/w$) and $k_B T_0$ ($\propto A_e \phi^{3/2}/w^2$) can be regarded, respectively, as the measure of energy required for an electron to cross the barrier and the energy well below which fluctuation effects become insignificant (here ϕ is the effective potential barrier height and w is the effective potential barrier width). By fitting the measured $G(T)$ behaviour to equation (1), one can obtain the values of T_1 and T_0.

(ii) At high bias voltages V_h (i.e. the nonlinear regime), the FITC theory delineates the $I(V)$ curve for $|V_h| < V_{hc}$ in the form [22, 23]

$$I_h(V_h, T) = I_{hs} \exp[-a(1 - V_h/V_{hc})^2], \qquad (2)$$

where the saturation current I_{hs} and the critical voltage V_{hc} are parameters that depend only weakly on T, and the parameter $a = T_1/(T_0 + T)$ describes the thermal effect on the $I_h(V_h)$ curves. Note that the ohmic regime at low bias voltages is not included in the derivation of equation (2). Therefore, the $G_F(T)$ behaviour (equation (1)) cannot be derived from equation (2) by simply taking the $V_h \to 0$ limit of $(\mathrm{d}I_h/\mathrm{d}V_h)^{-1}$. The value of a at each T can be first extracted by fitting the measured $I_h(V_h)$ curve to equation (2). Then, by further fitting the obtained a values to $T_1/(T_0 + T)$, an alternative set of values of the same parameters T_1 and T_0 can be determined.

Thus, by means of these two complementary methods, one can perform a quantitative self-consistent check of the FITC theoretical predictions by comparing the two sets of the extracted T_1 and T_0 values.

Figure 3 shows the log–log plot of $G/G_{F\infty}$ as a function of T for the six TJs. The solid curves are the fits to equation (1) with $G_{F\infty}$, T_1, and T_0 as the fitting parameters. Reasonable agreement is obtained between equation (1) and our data. The inset shows a semi-log plot of $G_{F\infty}$ versus T_1/T_0 extracted from the fits. Table 1 lists the values of the relevant parameters for the six TJs. The values are similar to those obtained in our previous works [13, 24, 25]. In the FITC theory, $T_1/T_0 \propto w\phi^{1/2}$, which reflects the effective potential barrier shape and therefore prescribes the $G_F(T)$ behaviour. For a series of TJs properly processed, a larger value of T_1/T_0 could correspond to a barrier with a larger value of either ϕ or w, provided that the other one is barely changed. In both cases, a smaller value of $G_{F\infty}$ can be derived. In this study, since the barrier underwent

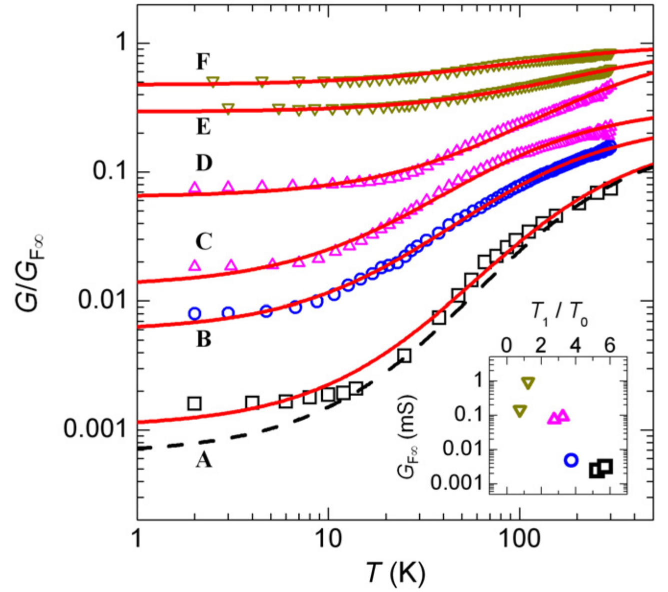

Figure 3. Log–log plot of $G/G_{F\infty}$ versus T for the six TJs. The solid curves are the fits to equation (1). The dashed curve through TJ A is the prediction of equation (1) but plotted with the T_1 and T_0 values extracted from a through equation (2). For clarity, the data for TJs A, B and C are divided by 5, 4 and 3, respectively. Inset: a semi-log plot of the fitted $G_{F\infty}$ values versus the fitted T_1/T_0 values.

Table 1. Values of the relevant parameters for the six TJs.

TJ	Method	$G_{F\infty}$ (mS)	T_1 (K)	T_0 (K)	T_1/T_0
A	$G_F(T)$	2.4×10^{-3}	310	59	5.3
	$I_h(V_h, T)$	3.2×10^{-3}	334	58	5.8
B	$G_F(T)$	4.9×10^{-3}	168	45	3.7
C	$G_F(T)$	8.9×10^{-2}	127	39	3.3
D	$G_F(T)$	7.4×10^{-2}	325	118	2.8
E	$G_F(T)$	9.3×10^{-1}	223	182	1.2
F	$G_F(T)$	1.4×10^{-1}	63	84	0.8

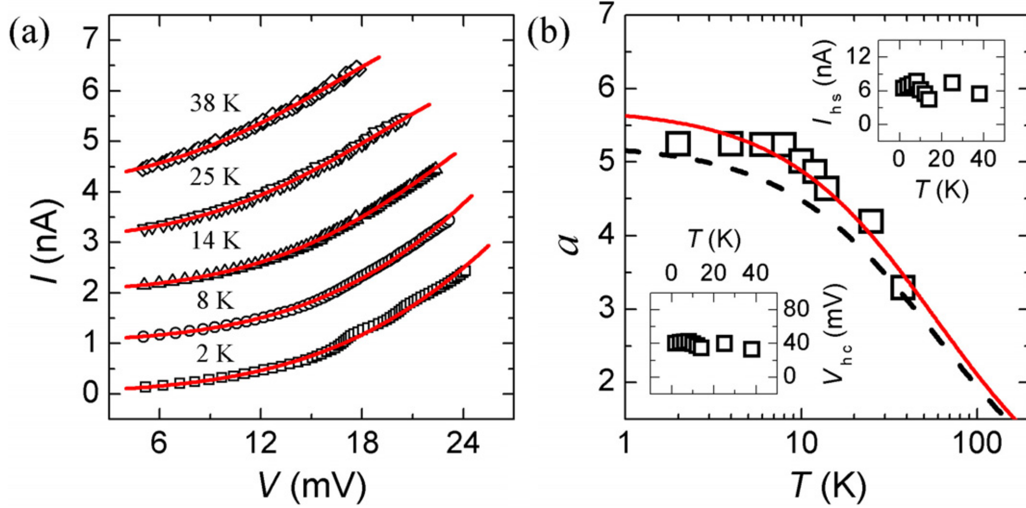

Figure 4. For TJ A. (*a*) Nonlinear $I(V)$ curves at five temperatures. The solid curves are the fits to equation (2). For clarity, the data for 8 K, 14 K, 25 K and 38 K are shifted upwards by 1 nA, 2 nA, 3 nA and 4 nA, respectively. (*b*) The extracted a values versus T. The solid curve is the fit to $T_1/(T_0+T)$. The dashed curve is the prediction of $T_1/(T_0+T)$ but plotted with the T_1 and T_0 values extracted from the fit to equation (1). Insets: the corresponding (top) $I_{hs}(T)$ and (bottom) $V_{hc}(T)$ plots.

an alteration that is essentially physical, ϕ (a property of the AlO_x layer) can be considered nearly unchanged. An increase of $G_{F\infty}$ with decreasing T_1/T_0 thus implies a decrease in w, which is expected when the ion milling technique is employed. In our previous work [25], such a trend was not clear as the nature of the insulator was not known. It should be noted that this argument could be inapplicable if the chemistry of the barrier has been considerably changed during the erosion process. In that case, the variation of $G_{F\infty}$ with T_1/T_0 might imply a different scenario. A detailed sputter-depth profiling of the barrier should be of value regarding this issue.

The self-consistency of the FITC description was checked for TJ A. In figure 3, the dashed curve through TJ A is the prediction of equation (1) plotted by directly substituting those T_1 and T_0 values inferred from the a values through equation (2) (i.e. $G_{F\infty}$ is the sole fitting parameter). The result is seen to describe the $G(T)$ behaviour of TJ A reasonably well. Figure 4(*a*) shows the measured nonlinear $I(V)$ curves for TJ A at five temperatures. The solid curves are the fits to equation (2). Good agreement between equation (2) and our data is evident. The extracted values of a as a function of T are plotted in figure 4(*b*), together with the fit (the solid curve) to $T_1/(T_0+T)$. In the insets, we plot the variations of the fitted I_{hs} and V_{hc} values with T. Note that they are almost independent of T, as expected under the FITC theory. Similarly, in figure 4(*b*), we plot the value of a (the dashed curve) calculated using those T_1 and T_0 values extracted from the $G(T)$ fit (equation (1)). Again, it is apparent that good agreement between equations (1) and (2) is found.

This consistency provides strong support for the relevance of the FITC process to electron transport in our TJs. The manifestation of this process at the micrometre scale directly reflects the presence of hot spots due to large junction–barrier interfacial roughness. As discussed previously [13, 26], these fine structures could be (or evolve into) nanoconstrictions whose transverse dimensions are less than half the Fermi wavelength. Owing to the continued miniaturization of devices, such atomic-scale fine structures could be of interest in applications such as emerging resistive switching elements [27]. This work therefore suggests accelerated ions to be a potential means to design relevant experiments.

The bombardment of the barrier with energetic ions may create additional electron states at the junction–barrier interface or inside the barrier, both of which can give exponential-like behaviour similar to that in figure 1(*a*). However, we consider that their contributions can be ignored in our TJs, for reasons discussed below. (i) Surface states can tilt the potential barrier shape to some extent [15] and very likely render the effective height much lower [28]. In this case, most of the electrons are thermionically emitted over, rather than tunnel through, the barrier at higher temperatures, exhibiting a behaviour given by [29] $G_{te}(T) \propto T\exp(-T_{te}/T)$, where T_{te} is a junction parameter. Figure 5(*a*) shows the variation of $\log[G/G(2\,\mathrm{K})T]$ with T^{-1} for the six TJs. Although linear regimes seem to exist at $T \approx$ 30–100 K (the grey area) in some of the TJs, the downward behaviour in all the TJs with further increasing T clearly cannot be accommodated by this model. (ii) Defect states inside the barrier can serve as a channel for electrons to hop via Mott's $T^{-1/4}$ law [30]: $G_M(T) \propto \exp[-(T_M/T)^{1/4}]$, where T_M is a characteristic temperature. This is valid when d is larger than the typical length of a hop ℓ ($\propto (T_M/T)^{1/4}$). As T decreases, $\ell \to d$, and a crossover to a much weaker T dependence (e.g., direct or resonant tunnelling) may occur [14]. Figure 5(*b*) shows the variation of $\log[G/G(2\,\mathrm{K})]$ with $T^{-1/4}$ for the six TJs. Linear regimes are found in all the TJs when T is higher than ~20 K (the grey area), below which G becomes saturated. For TJ A, the obtained $T_M^{1/4}$ value is ≈5 times larger than that for TJ F, meaning that the crossover (if it exists) in TJ A should occur at a temperature much higher than that in TJ F. However, this is inconsistent with the trend revealed in figure 5(*b*). Indeed, the occurrence of variant hopping processes through a barrier of $d \lesssim 2$ nm is highly questionable. (By the same token, our data

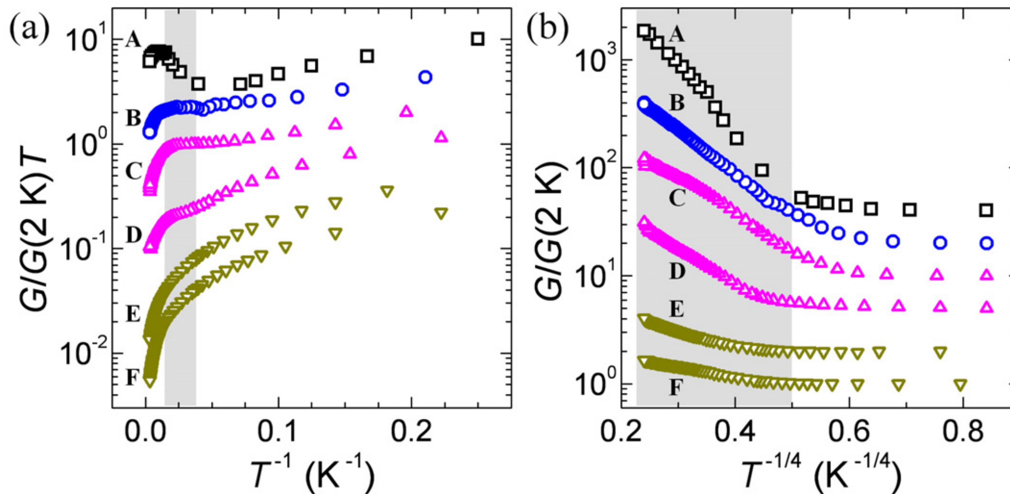

Figure 5. Semi-log plots of (*a*) $G/G(2\,\text{K})T$ versus T^{-1} and (*b*) $G/G(2\,\text{K})$ versus $T^{-1/4}$ for the six TJs. For clarity, the data for TJs A, B, C, D and E are multiplied by 40, 20, 10, 5 and 2, respectively.

cannot be explained in terms of the Efros–Shklovskii variable-range-hopping conduction process [31] (not shown).)

4. Conclusions

In summary, the effect of ion-milled barriers on electron transport in micrometre-sized all-Al TJs has been studied over a wide T range of 2–300 K. The measured $G(T)$ behaviour and the nonlinear $I(V)$ curves are found to be best described by the FITC mechanism, which signifies the presence of nanoscopic incomplete pinholes inside the barrier due to large junction–barrier interfacial roughness. This topographical feature has also been observed in the cross-sectional TEM image of the TJ stack with an ion-milled barrier. We have demonstrated that the use of low energy Ar-ion beams for reducing the barrier thickness not only roughens the barrier but also substantially affects the electron tunnelling behaviour. Our results are important when considering the behaviour of tunnel devices in which ion-milling techniques are employed to tune barrier properties.

Acknowledgments

The authors are grateful to Ping Sheng for helpful discussions. This work was supported by the Taiwan National Science Council through grant numbers NSC 101-2112-M-018-004-MY3 (JCW), NSC 102-2120-M-009-003 (JJL) and by the MOE ATU Program (JJL).

References

[1] Moeckly B H and Char K 1997 *Appl. Phys. Lett.* **71** 2526
[2] Grossman E N, Harvey T E and Reintsema C D 2002 *J. Appl. Phys.* **91** 10134
[3] Schmalhorst J and Reiss G 2003 *Phys. Rev.* B **68** 224437
[4] Huang J C A, Hsu C Y, Liao Y F, Lin M Z and Lee C H 2005 *J. Appl. Phys.* **98** 103504
[5] Pomeroy J M, Grube H, Perrella A C and Gillaspy J D 2007 *Appl. Phys. Lett.* **91** 073506
[6] Egelhoff W F Jr, Höink V E, Lau J W, Shen W F, Schrag B D and Xiao G 2010 *J. Appl. Phys.* **107** 09C705
[7] Baklanov M R, de Marneffe J F, Shamiryan D, Urbanowicz A M, Shi H, Rakhimova T V, Huang H and Ho P S 2013 *J. Appl. Phys.* **113** 041101
[8] Lee H M, Lee Y C, Chen H H, Horng L, Wu J C, Lee C M, Wu T H and Chern G 2012 *Spin* **2** 1230002
[9] Ziberi B, Frost F, Höche Th and Rauschenbach B 2005 *Phys. Rev.* B **72** 235310
[10] Da Costa V, Tiusan C, Dimopoulos T and Ounadjela K 2000 *Phys. Rev. Lett.* **85** 876
[11] Buchanan J D R, Hase T P A, Tanner B K, Hughes N D and Hicken R J 2002 *Appl. Phys. Lett.* **81** 751
[12] Cruz de Gracia E S, Dorneles L S, Schelp L F, Teixeira S R and Baibich M N 2007 *Phys. Rev.* B **76** 214426
[13] Lai Y R, Yu K F, Lin Y H, Wu J C and Lin J J 2012 *AIP Adv.* **2** 032155
[14] Xu Y, Ephron D and Beasley M R 1995 *Phys. Rev.* B **52** 2843
[15] Jung H, Kim Y, Jung K, Im H, Pashkin Yu A, Astafiev O, Nakamura Y, Lee H, Miyamoto Y and Tsai J S 2009 *Phys. Rev.* B **80** 125413
[16] Lacquaniti V, Belogolovskii M, Cassiago C, De Leo N, Fretto M and Sosso A 2012 *New J. Phys.* **14** 023025
[17] Freericks J K 2004 *Appl. Phys. Lett.* **84** 1383
[18] Li B, Miao G X and Moodera J S 2013 *Phys. Rev.* B **88** 161105
[19] Joo S, Jung K Y, Lee B C, Kim T S, Shin K H, Jung M H, Rho K J, Park J H, Hong J and Rhie K 2012 *Appl. Phys. Lett.* **100** 172406
[20] Simmons J G 1963 *J. Appl. Phys.* **35** 2655
[21] Ditchfield R and Seebauer E G 2001 *Phys. Rev.* B **63** 125317
[22] Sheng P, Sichel E K and Gittleman J I 1978 *Phys. Rev. Lett.* **40** 1197
[23] Sheng P 1980 *Phys. Rev.* B **21** 2180
[24] Lin Y H and Lin J J 2011 *J. Appl. Phys.* **110** 064318
[25] Lin Y H, Chiu S P and Lin J J 2008 *Nanotechnology* **19** 365201
[26] Xie H and Sheng P 2009 *Phys. Rev.* B **79** 165419
[27] Pershin Y V and Di Ventra M 2011 *Adv. Phys.* **60** 145
[28] Im H, Pashkin Yu A, Yamamoto T, Astafiev O, Nakamura Y and Tsai J S 2006 *Appl. Phys. Lett.* **88** 112113
[29] Sze S M and Ng K K 2007 *Physics of Semiconductor Devices* 3rd edn (Hoboken, NJ: Wiley-Interscience)
[30] Mott N F and Davis E A 1979 *Electronic Processes in Non-Crystalline Materials* 2nd edn (New York: Oxford University Press)
[31] Shklovskii B I and Efros A L 1984 *Electronic Properties of Doped Semiconductors* (Berlin: Springer)